# Theoretical Study of Formamide Decomposition Pathways

**ARTICLE** *in* THE JOURNAL OF PHYSICAL CHEMISTRY A · FEBRUARY 2011

Impact Factor: 2.69 · DOI: 10.1021/jp109143j · Source: PubMed



**6 AUTHORS**, INCLUDING:

Nguyen Vinh Son
University of Leuven
**35** PUBLICATIONS **488** CITATIONS
SEE PROFILE

T. M. Orlando
Georgia Institute of Technology
**197** PUBLICATIONS **2,733** CITATIONS
SEE PROFILE

Minh Tho Nguyen
University of Leuven
**748** PUBLICATIONS **10,835** CITATIONS
SEE PROFILE

THE JOURNAL OF PHYSICAL CHEMISTRY A

ARTICLE

pubs.acs.org/JPCA

# Theoretical Study of Formamide Decomposition Pathways

Vinh Son Nguyen,[†] Heather L. Abbott,[*,‡] M. Michele Dawley,[‡] Thomas M. Orlando,[‡] Jerzy Leszczynski,[§] and Minh Tho Nguyen[*,†]

[†]Department of Chemistry, and LMCC-Mathematical Modeling and Computational Science Center, Katholieke Universiteit Leuven, B-3001 Leuven, Belgium

[‡]School of Chemistry and Biochemistry, Georgia Institute of Technology, Atlanta, Georgia 30332-0400, United States

[§]Interdisciplinary Center for Nanotoxicity, Department of Chemistry, Jackson State University, Jackson, Mississippi 39217-0510, United States

Supporting Information

**ABSTRACT:** The chemical transformations of formamide ($NH_2CHO$), a molecule of prebiotic interest as a precursor for biomolecules, are investigated using methods of electronic structure computations and Rice−Rampserger−Kassel−Marcus (RRKM) theory. Specifically, quantum chemical calculations applying the coupled-cluster theory CCSD(T), whose energies are extrapolated to the complete basis set limit (CBS), are carried out to construct the [$CH_3NO$] potential energy surface. RRKM theory is then used to systematically examine decomposition channels leading to the formation of small molecules including CO, $NH_3$, $H_2O$, HCN, HNC, $H_2$, HNCO, and HOCN. The energy barriers for the decarboxylation, dehydrogenation, and dehydration processes are found to be in the range of 73−78 kcal/mol. $H_2$ loss is predicted to be a one-step process although a two-step process is competitive. CO elimination is found to prefer a two-step pathway involving the carbene isomer $NH_2CHO$ (aminohydroxymethylene) as an intermediate. This CO-elimination channel is also favored over the one-step $H_2$ loss, in agreement with experiment. The $H_2O$ loss is a multistep process passing through a formimic acid conformer, which subsequently undergoes a rate-limiting dehydration. The dehydration appears to be particularly favored in the low-temperature regime. The new feature identifies aminohydroxymethylene as a transient but crucial intermediate in the decarboxylation of formamide.

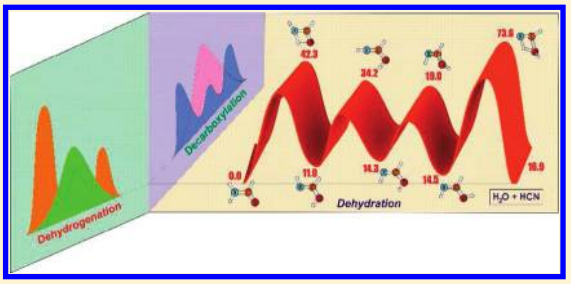


## 1. INTRODUCTION

Formamide ($NH_2CHO$, denoted hereafter as FM) has been considered an active key precursor in prebiotic Earth chemistry leading to more complex biomolecules.[1−4] It also has been tentatively identified in interstellar ices,[5] in the long-period comet C/1995 O1 Hale-Bopp,[6] and in the protostellar source NGC 7538 IRS9.[7] These findings have fueled interest in FM's role in the formation of more complex molecules such as amino acids on interstellar icy grains.[8] Further consideration of FM's role arises from its unique chemical properties. FM is the lowest energy isomer of the [$CH_3NO$] compounds and the simplest stable organic species having the four most common elements. FM is the simplest member of the amide functional group, which contains the prototypical NH—C═O linkage in peptides. This linkage is reactive at both amino and carbonyl sites and is expected to constitute a key building block for formation of nucleic acids. FM is also a likely precursor for nucleobases because of its relative stability, low volatility compared to water, versatile reactivity, and likely prebiotic availability.[9] Indeed, formation of amino acids by thermal decomposition of FM has been reported to occur via oligomerization of HCN,[10] and formation of DNA nucleobases (e.g., adenine, hypoxanthine, and guanine) from heated and UV-irradiated neat FM solutions has recently been demonstrated.[9]

Previous experimental results on thermal FM decomposition are briefly summarized. Back and Boden[11] showed that in the relatively slow thermal decomposition of the FM vapor which accompanied the high-temperature photolysis, CO and $NH_3$ were observed as major products and $H_2$ as a minor product. These authors reported that rates of production of CO and $H_2$ were approximately first-order in FM pressure and were given by the rate constants of $k_{CO}/s^{-1} = 3.9\ \exp((-15000\ \text{cal/mol})/RT)$ and $k_{H_2}/s^{-1} = 0.30\ \exp((-15000\ \text{cal/mol})/RT)$. Since the CO elimination was about 13 times faster than the $H_2$ loss, an interface phenomenon rather than a gas-phase reaction was suggested. Kakumota et al.[12] studied the thermal decomposition of FM diluted in Ar using shock-tube experiments over the temperature range of 1690−2180 K, and the rate was monitored by means of infrared (IR) emission of the CO produced. Decomposition proceeded in the decarbonylation channel in

**Received:** September 24, 2010
**Revised:** December 15, 2010
**Published:** January 13, 2011

the falloff region. From the falloff data and inputs from ab initio calculations of structures, the rate constants were determined to be $k_{CO}(\infty)/s^{-1} = 10^{14.02}\ \exp((-75.5\ \text{kcal/mol})/RT)$ in the high-pressure limit. Okazaki and Funazukuri[13] carried out FM decomposition in pressurized hot water in a tubular flow reactor at 573−693 K and a pressure of 23 MPa. The major products were $NH_3$ and CO. The latter underwent subsequent reaction with water producing formic acid. Caltado et al. prolonged the heating of FM and monitored the volatile products that evolved using gas-phase IR spectroscopy.[14] The gaseous products released from FM included CO, $CO_2$, and $NH_3$ at 185 °C; HCN also was detected due to dehydration of FM at 220 °C.

Theoretical studies have also explored portions of the potential energy surface for $[CH_3NO]$ using ab initio electronic structure methods for different reactive channels, including reactions of ionized formamide and reactions with water.[15−20] In spite of the large number of investigations available, the molecular mechanisms associated with the complete transformations of FM and some of its low-energy isomers are not fully understood. Previous studies have revealed that the $H_2$ and CO losses are elementary processes, if they occur in the ground state of neutral FM.[18] Photochemical elimination of $H_2$ has been proposed to occur in the lowest lying triplet state of neutral FM involving a two-step process.[20] However, Peterson et al.'s femtosecond study of the photolysis of aqueous FM showed that the majority of excited FM molecules return to the ground state within the first picosecond after excitation.[21] A relatively slow thermal decomposition vapor was found to accompany FM high-temperature photolysis.[11] Overall, these results suggest that FM decomposition may occur in its ground electronic state, even when the sample is UV irradiated. Thus, it can be expected that the "hot" FM ground-state molecule, once generated in a vibrationally excited but electronically deactivated state, undergoes unimolecular rearrangements that are different from the one-step dissociation channels. While $H_2$ and CO could, in principle, be directly formed from FM, generation of $H_2O$ cannot be accomplished in a one-step process and thus requires rearrangements.[22] Therefore, it is imperative to consider the possible involvements of the numerous lower lying tautomers.

A comprehensive theoretical search for intermediate isomers that could play an important role in the transformation of FM has not been fully executed. Only small and disparate portions of the potential energy surface have been explored, using different levels of theory.[16,18−20,23] This does not allow a consistent comparison of the reaction energetics. Therefore, this paper details a systematic exploration of the FM decomposition in the lowest lying singlet manifold, making use of high-accuracy electronic structure calculations. Possible unimolecular transformations of FM into numerous decomposition products include $NH_3 + CO$, $H_2O + HCN$ (or HNC), and $H_2 + HNCO$ (or HCNO, HOCN, HCON, HNOC). Here, we have explored all of these reaction pathways and have chosen to focus our discussion on the five decomposition processes presented in Figure 1. Overall, complete construction of the $[CH_3NO]$ potential energy surface provides the relative stabilities of isomeric systems and the energy barriers for different rearrangements and decompositions. Also, this approach can identify new energy reaction pathways and thereby novel molecular mechanisms. Ab initio quantum chemical calculations are expected to provide thermochemical parameters of small-size organic compounds with high accuracy, up to ±1.0 kcal/mol on heats of formation of equilibrium structures and ±2.0 kcal/mol on activation energies.[24,25]

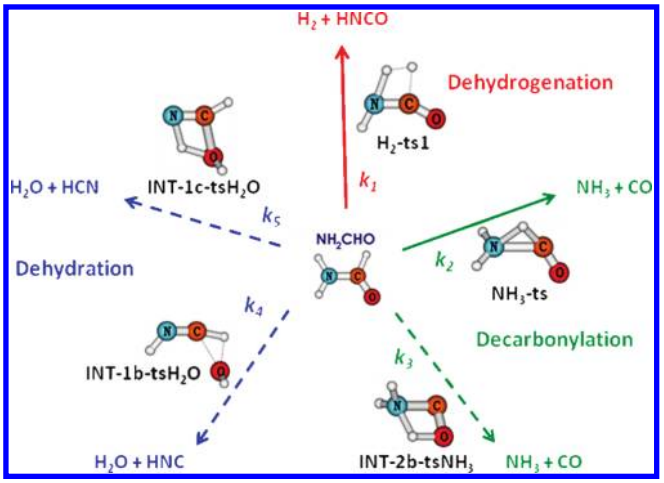


**Figure 1.** Possible reaction channels and products of the unimolecular decomposition of formamide. Solid arrows designate one-step unimolecular decay, while dashed arrows indicate multistep decomposition. Each arrow is labeled with the relevant Rice−Ramsperger−Kassel−Marcus (RRKM) rate constant. The transition-state structures are shown for each reaction pathway used in RRKM calculations of the rate constants, $k_i$.

The kinetic parameters of various channels can subsequently be evaluated using calculated geometric, vibrational, and energetic results. Calculated vibrational spectra could also be helpful in the identification of new or unknown species.

## 2. METHODS

**2.1. Electronic Structure Methods.** The electronic structure calculations are performed using the Gaussian 03[26] and Molpro[27] suite of programs. Geometries of the equilibrium and transition structures on the $[CH_3NO]$ potential energy surface are fully optimized, and corresponding rotational constants and harmonic vibrational frequencies are calculated using molecular orbital theory at the second-order perturbation MP2 level with the correlation-consistent aug-cc-pVDZ basis set. Geometries of the relevant structures are subsequently reoptimized at the MP2 level with the larger aug-cc-pVTZ basis set. For some open-shell species, the fully unrestricted formalism (UHF, UMP2) is used with Gaussian 03. Single-point electronic energies are calculated using the coupled-cluster theory CCSD(T) formalism,[28,29] in conjunction with the correlation-consistent aug-cc-pVnZ (n = D, T, and Q) basis sets,[30,31] using (U)MP2/aug-cc-pVTZ optimized geometries. For simplicity, the basis sets are denoted hereafter as aVnZ. The CCSD(T) energies are extrapolated to the complete basis set (CBS) limit energies using the following expression:[32]

$$E(x) = A_{CBS} + B\exp[-(x-1)] + C\exp[-(x-1)^2] \quad (1)$$

Although, one can extrapolate the HF and correlation energies separately, this does not substantially improve the fits. The relative energies between stationary points on the different pathways are then obtained from CCSD(T)/CBS total energies and corrected for the zero-point vibrational energy (ZPE) contributions. The ZPE values are obtained from MP2/aVDZ harmonic vibrational frequencies.

**2.2. Transition-State Theory.** Rice−Ramsperger−Kassel−Marcus (RRKM) theory is employed to evaluate rate constants for the key reaction pathways schematically depicted in Figure 1.[33,34]

All calculations are performed using self-developed code in Wolfram Mathematica 7.[35] Reaction rates are calculated using the general formula

$$k(T,p) = \int_0^\infty \frac{k_p\, k(E)}{k_p + k(E)} f(E)\, dE \quad (2)$$

We employ RRKM rate constants of the form

$$\frac{k(E) = N^{\ddagger}(E - E_0)}{(h\rho(E))} \quad (3)$$

where $N^{\ddagger}(E-E_0)$ is the sum of states for the reactive transition state, $\rho(E)$ is the density of states for the reactant, and $h$ is Planck's constant. Canonical probability distributions for each degree of freedom (i.e., translation, vibration, and rotation) are convolved such that an energy- and temperature-dependent probability distribution for the reactants is formed:

$$f(E) = \int_0^E f_t(E_t) \int_0^{E-E_t} f_v(E_v)\, f_r(E - E_t - E_v)\, dE \quad (4)$$

Pressure dependence is accounted for using the term $k_p = \beta Z_{LJ}[M]$, where $\beta$ is the collision efficiency coefficient, $Z_{LJ}$ is the Lennard-Jones collision frequency, and [M] can be computed from the ideal gas law as (i.e., $[M] = p/RT$). In this work, we assume $\beta \approx 1$ (i.e., strong collisions) and $Z_{LJ}[M] \approx 10^{10}$ for $p = 1$ atm.[36] (Note: In the high-pressure limit, we assume $k(T) = \int_0^\infty k(E)\, f(E)\, dE$.[34]) Rotational degrees of freedom are treated classically, and the vibrational sum/density of states are performed using the Beyer−Swinehart−Stein−Rabinovitch (BSSR) direct count algorithm. Reaction threshold energies ($E_0$) are taken from CCSD(T)/CBS calculations, wheras harmonic vibrational modes and rotational constants are obtained from electronic structure calculations at the MP2/aug-cc-pVTZ level.

## 3. RESULTS AND DISCUSSION

Structure and basic spectroscopic parameters of FM have been well-established.[37] Optimized geometries of FM and various lower lying [$CH_3NO$] isomers have been reported and abundantly analyzed in the literature.[16,18−20,23] Therefore, they warrant no additional comments. The Cartesian coordinates of the optimized geometries of all isomers using the MP2/aug-cc-pVTZ method are listed in Table S1 of the Supporting Information (ESI). The relative energy values of the isomers and transition structures (TS) that are given in different energy profiles are obtained, unless otherwise stated, using CCSD(T)/CBS + ZPE calculations. As a convention, each structure considered is labeled by a combination of letters and numbers, in which the letters ts stand for a transition structure connecting two equilibrium structures. Identity of each ts can easily be determined. In some more ambiguous cases, intrinsic reaction coordinate (IRC) calculations are carried out to establish the connection.

**3.1. One-Step Reaction Channels from Formamide.** We first consider the one-step decompositions of the neutral FM. Figure 2 schematically displays the calculated energy profiles illustrating a competition between (A) the decarbonylation $NH_2CHO \rightarrow CO + NH_3$ via TS $NH_3$-ts and (B) the dehydrogenations $NH_2CHO \rightarrow H_2 + HNCO$ via two TSs, $H_2$-ts1 and $H_2$-ts2. In Figure 2 and also in the following figures, FM is denoted by $NH_2CHO$. Normally, the different product fragments derived from these reactions, once generated, form weak

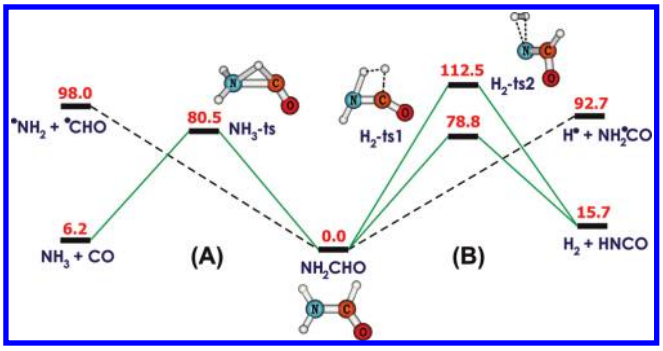


**Figure 2.** Schematic energy profiles illustrating the one-step decomposition channels of formamide. Relative energies given in kilocalories per mole are obtained from CCSD(T)/CBS + ZPE calculations.

H-bonded complexes such as CO−$NH_3$ and $H_2$−HNCO. These weak complexes, whose formation energies are a few kilocalories per mole, have been detected in low-temperature matrix experiments. However, they are not important for an understanding of the decomposition mechanism and are omitted in the following energy profiles.

The calculated reaction energy of 6.2 kcal/mol for A is close to the experimental value of 6.6 kcal/mol, evaluated from experimental standard heats of formation.[51] In contrast, the CBS value of 15.7 kcal/mol for B does not compare well with the experimental counterpart of 19.0 kcal/mol, which is based on the value $\Delta H_f$(HNCO) = −24.8 ± 2.8 kcal/mol (298 K).[38] However, the error bar of ±2.8 kcal/mol on the experimental value is rather large. Martell et al. used density functional theory and molecular orbital calculations up to the G2 level. The G2 result of 15.8 kcal/mol for the reaction energy is nearly identical to our new CBS value.[18] The N−H and C−N bond cleavages turn out to be much less favored (Figure 2). The courses of both reactions A and B have been examined in detail in previous theoretical studies; however, these disagreed with each other on the relative ordering of the energy barriers.[18,20] At the G2 level, the energy barriers were calculated to be 80.7 and 78.3 kcal/mol for decompositions A and B, respectively.[18] In contrast, Li et al. constructed multiconfigurational wave functions at the CASPT2/CASSCF(6,6)/6-31G(d,p) level and obtained a reversed ordering of the two barriers, namely, 74.9 and 85.0 kcal/mol for A and B, respectively.[20] Our CBS results appear to agree with the previous and lower level G2 values. The barrier for dehydrogenation of 78.8 kcal/mol through $H_2$-ts1 is slightly smaller than that for decarbonylation of 80.5 kcal/mol via $NH_3$-ts (Figure 2). The sharp difference of CASPT2 results likely arises from an unbalanced treatment of the nondynamic correlation energies due to the difference in the selected active spaces for CASSCF wave functions. We note that the DFT/B3LYP method yields the same energy ordering for both barriers as with the G2 or CBS methods, even though the absolute density functional theory (DFT) values are ∼3 kcal/mol smaller than the CBS counterparts.

The geometrical features of both transition structures have been well-analyzed.[18,20] Proceeding along the reverse reaction, $NH_3$-ts corresponds to an insertion of the CO into an N−H bond of ammonia. This is basically a nucleophilic addition involving an interaction between the carbon lone pair (HOMO) with a vacant $\sigma^*$(N−H) orbital (LUMO). In contrast, the dehydrogenation is a classical 1,2-$H_2$ elimination through a four-membered TS, $H_2$-ts1.


dx.doi.org/10.1021/jp109143j |J. Phys. Chem. A 2011, 115, 841–851

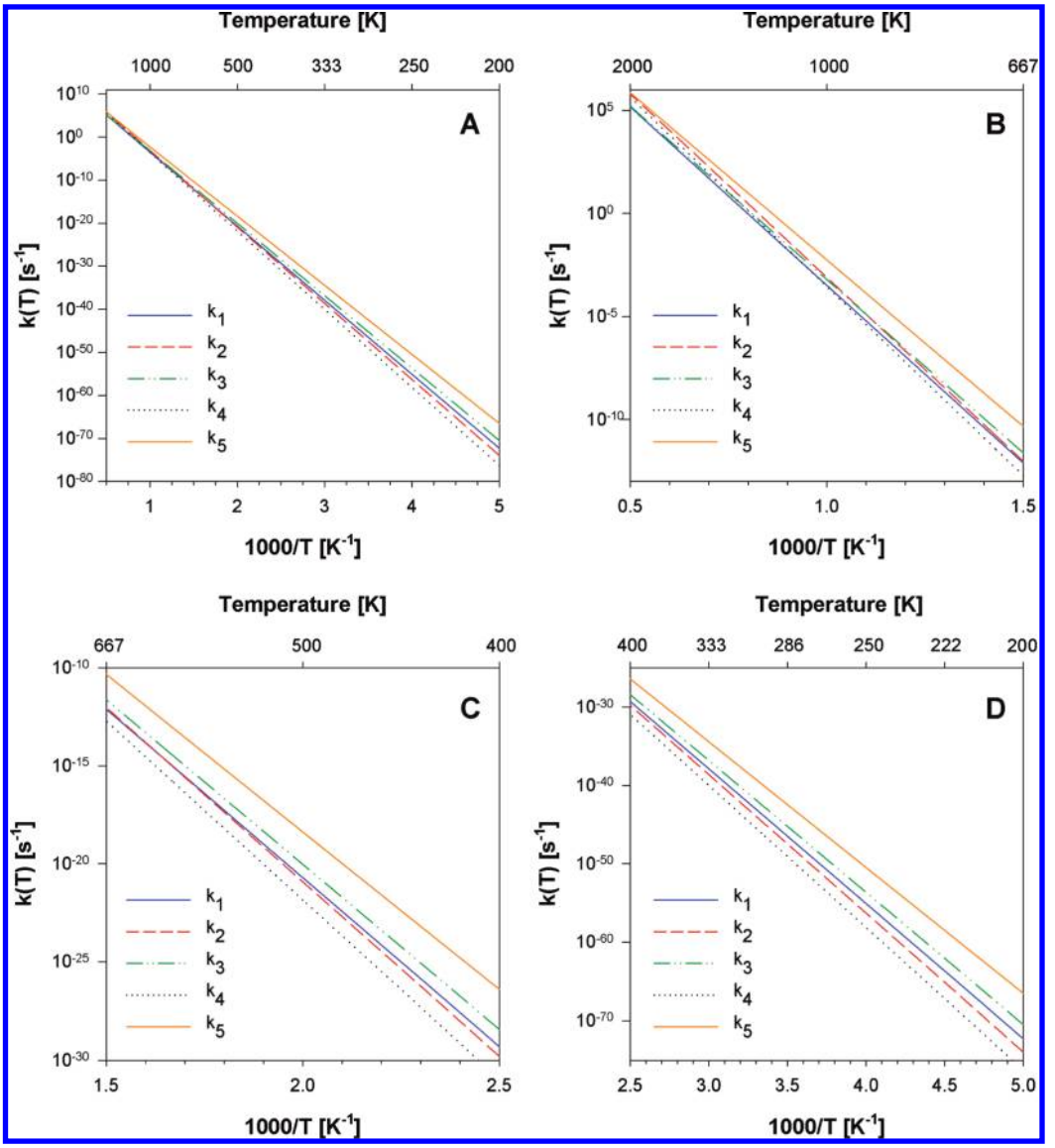


**Figure 3.** Variations of the apparent rates for reaction pathways in the high-pressure limit are shown over the entire temperature range (A; 200−2000 K). For clarity, the plot has also been separated into high-temperature (B; 667−2000 K), intermediate-temperature (C; 400−667 K), and low-temperature (D; 200−400 K) regions.

The 1,1-$H_2$ elimination from the amino group also proceeds through $H_2$-ts2, but this process requires a substantial activation energy which is even larger than the homolytic bond dissociation energies (cf. Figure 2). This is due to the instability of the product formylnitrene (HCON) being unstable in the singlet state. Note that formation of the carbamyl ($NH_2CO$) radical was detected in high-temperature photolysis of FM, which undergoes further decomposition yielding $NH_2$ and CO.[11]

To compare the one-step dehydrogenation ($k_1$) and decarbonylation ($k_2$) more thoroughly, we have computed RRKM rate constants on the basis of the transition-state structures shown in Figure 1 (coordinates given in ESI). In Figure 3, the evolution of rate constants as a function of temperature ($T$ = 200−2000 K) in the high-pressure limit is shown. The high-pressure-limit rates are fit to a general Arrhenius-type expression:

$$k_i(T) = AT^m e^{-E_a/k_B T} \quad (5)$$

and the best-fit parameters are given in Table 1.

**Table 1. Parameters for the Optimized General Expression of the Thermal Rate Constants in the High-Pressure Limit, $k(T) = AT^m \exp(-E_a/RT)$**

| | $A$ ($s^{-1}$) | $M$ | $E_a$ (kcal/mol) |
|---|---|---|---|
| $k_1$ | $4.71 \times 10^{13}$ | 0.262 | 78.5 |
| $k_2$ | $3.17 \times 10^{14}$ | 0.555 | 80.6 |
| $k_3$ | $4.16 \times 10^{13}$ | $-8.40 \times 10^{-3}$ | 77.0 |
| $k_4$ | $3.14 \times 10^{14}$ | 0.633 | 82.7 |
| $k_5$ | $5.69 \times 10^{13}$ | 0.355 | 73.3 |

As illustrated in Figure 3, one-step dehydrogenation is largely dominant over decarbonylation when $T$ < 600 K for all pressures considered. For example, $k_1 = 2.28 \times 10^{-44}$ $s^{-1}$ and $k_2 = 2.74 \times 10^{-45}$ $s^{-1}$ in the high-pressure limit at 300 K. (This is most clearly visible in Figure 3D.) At $T \sim 600$ K, dehydrogenation and decarbonylation have approximately equal branching ratios (cf., $k_1 = 1.05 \times 10^{-15}$ $s^{-1}$ and $k_2 = 1.00 \times 10^{-15}$ $s^{-1}$). Only


dx.doi.org/10.1021/jp109143j |J. Phys. Chem. A 2011, 115, 841–851

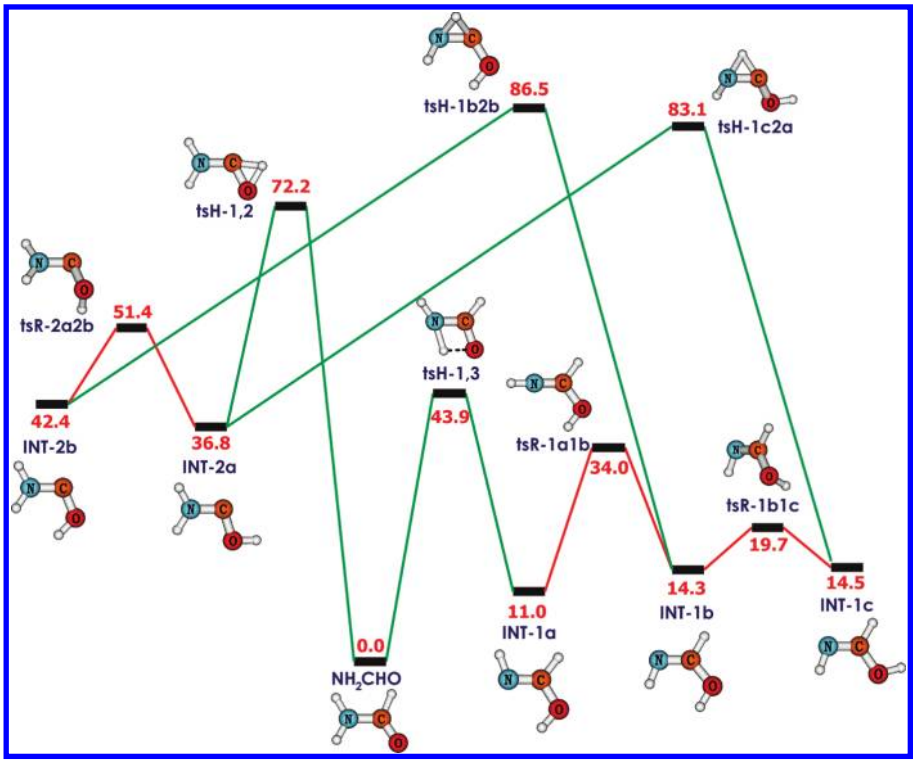


**Figure 4.** Schematic energy profiles illustrating the unimolecular rearrangements of formamide through 1,2-H and 1,3-H shifts, rotations, and inversions. Relative energies given in kilocalories per mole are obtained from CCSD(T)/CBS + ZPE calculations.

at $T > 600$ K does the kinetically favorable one-step decarbonylation pathway dominate the reactivity (cf., $k_1 = 3.24 \times 10^{-4}$ s$^{-1}$ and $k_2 = 7.78 \times 10^{-4}$ s$^{-1}$ at 1000 K). This finding suggests that at low temperatures the one-step dehydrogenation pathway will actually be dominant over the one-step decarbonylation pathway, in contrast to some experimental results.[11,12] As discussed further in section 3.2c, our calculations actually suggest that decarbonylation is a multistep process rather than single step reaction pathway.

All rate constants have also been calculated at pressures of 1.0, 0.1, and 0.01 atm and are plotted in Figures S1−S3 (ESI) of the Supporting Information. Figure S1 illustrates that the rate constants become somewhat larger as the pressure increases for a given temperature. This increase is more pronounced at higher temperatures (e.g., at 2000 K, $k_5 = 1.2 \times 10^5$ s$^{-1}$ for 0.01 atm while $k_5 = 7.1 \times 10^5$ s$^{-1}$ in the high-pressure limit). However, the ratio of the rate constants toward one another is essentially independent of the pressure as highlighted in Figures S2 and S3. The only exception to this is the relative ratio of $k_3$ to $k_4$. At high temperatures ($T = 800-2000$ K) and at the lowest pressure (0.01 atm), the ratio $k_3/k_4 > 1$ (i.e., $k_3 > k_4$), while at higher pressures (0.1 atm, 1 atm, and in the high-pressure limit) the ratio $k_3/k_4 < 1$ (i.e., $k_4 > k_3$). Thus, we conclude that the reaction pathways examined here show a negligible pressure dependence, in the low-temperature region of interest (i.e., $T <$ 800 K).

**3.2. Multistep Channels from Formamide to Isomers with N−C═O Framework. a. Interconversions between Low-Lying Isomers.** To further establish the possible decomposition channels, we explore the regions of the potential energy surface containing the numerous interconnections between FM and its immediate isomers that have the N−C−O connectivity. Figure 4 provides a summary of the potential energy profiles for the most relevant isomerizations. These rearrangements are mainly made through simple 1,2 and 1,3 shifts of one H atom moving around the three heavy atoms. As for a convention, each isomer is labeled as INT-xy, where INT stands for a local equilibrium structure and x is a number (1 and 2) indicating a different isomer, whereas y is a letter designating a different conformer of the same isomer. The interconnections between conformers occur via rotation around single bonds or inversion about the C═N double bond and are also shown in Figure 4. These processes are simple but important because decomposition often occurs only at a specific conformation. For the sake of simplification, the different channels arising from homolytic N−H, C−H, and O−H, etc., bond cleavages are omitted. These radical fragments are located at higher dissociation energy limits.

Figure 4 includes the energetics for interconnections leading to formimidic acid INT-1 (*C*-hydroxyimine) and aminohydroxycarbene INT-2. In its most stable conformer INT-1, INT-1a is 11.0 kcal/mol above FM, which is the lower lying isomer of the two. The FM−INT-1 tautomerization has been experimentally studied using UV irradiation of matrix-isolated FM in solid Ar. All rotamers were identified and characterized by IR spectroscopy.[22,39] The relative energies seen in Figure 4 concur with this observation. The 1,3-H shift from FM giving INT-1a is associated with an energy barrier of 43.9 kcal/mol through tsH-1,3. The barriers for N inversion and OH rotation are substantially smaller (Figure 4), and therefore the less stable conformers can also be generated from the activated FM molecule.

Aminohydroxycarbene INT-2 is calculated to be much less stable, being 36.8 kcal/mol above FM. Due to such low stability, the 1,2-H shift generating the carbene is an energetically demanding process, in which the associated TS tsH-1,2 is located at 72.2 kcal/mol. Thus under mild thermal conditions, formation of carbene is not competitive with that of formimidic acid. Figure 4


dx.doi.org/10.1021/jp109143j |*J. Phys. Chem. A* 2011, 115, 841–851

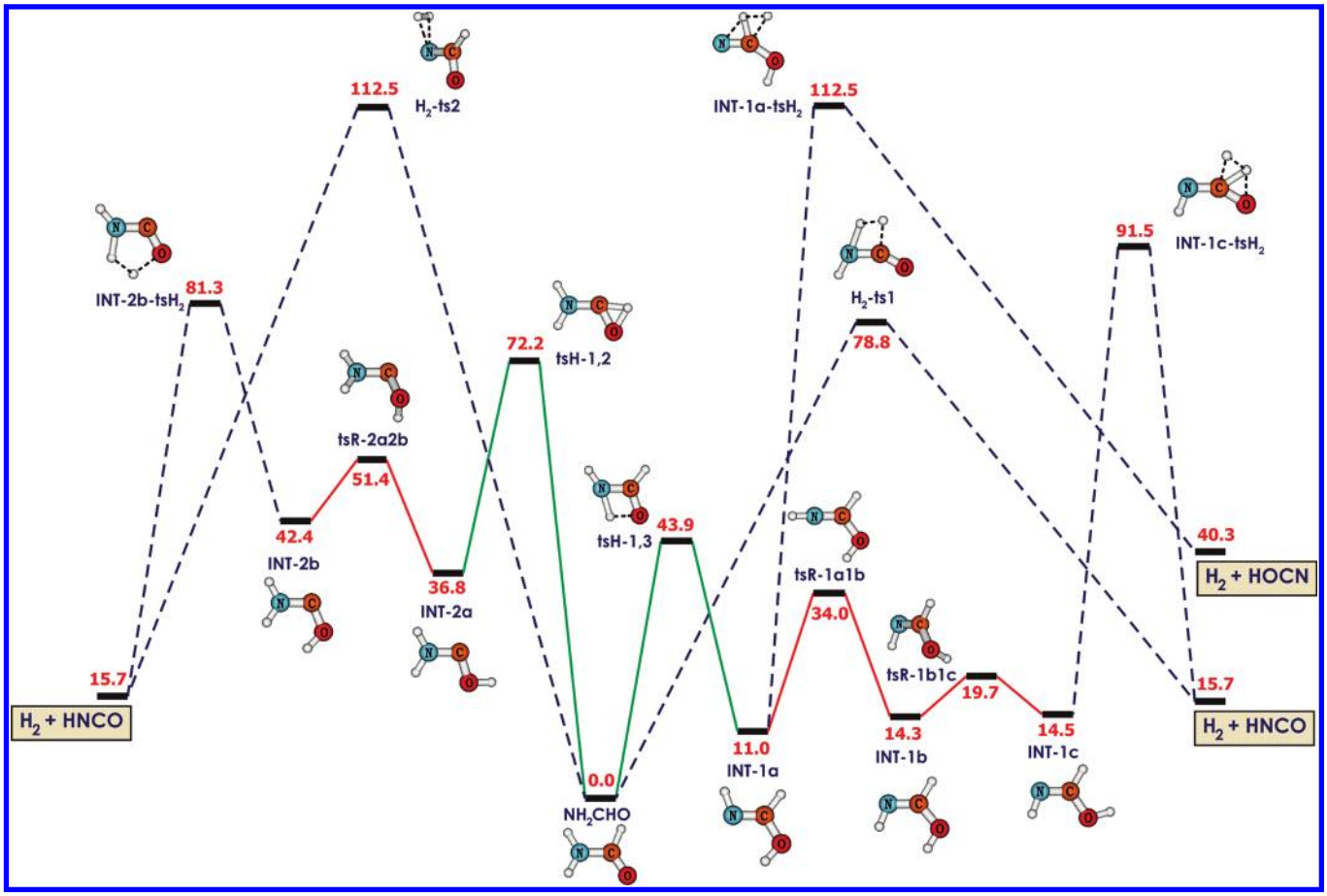


**Figure 5.** Schematic energy profiles illustrating the pathways leading to dehydrogenation of formamide. Relative energies given in kilocalories per mole are obtained from CCSD(T)/CBS + ZPE calculations.

also points out that direct interconversions between different conformers of both isomers INT-1 and INT-2 have energy barriers > 83 kcal/mol and do not compete with their rearrangement back to FM. Nevertheless, tsH-1,2 is located below the two TSs for one-step decomposition, $NH_3$-ts (80.5 kcal/mol) and $H_2$-ts1 (78.8 kcal/mol, Figure 2). Therefore it is instructive to explore further the behavior of both isomers with respect to unimolecular decomposition.

**b. Dehydrogenation from Two N−C−O Isomers.** Figure 5 displays the energy profiles showing the main dehydrogenation channels involving both isomers INT-1 and INT-2. For comparison, some relevant points given in Figure 4 are again included in Figure 5. A few results are noteworthy:

(i) The one-step $H_2$ loss from INT-1c, which is the least stable conformer but has the right atom arrangement for $H_2$ departure, occurs via INT-1c-ts$H_2$ and implies a large energy barrier. In their matrix photolysis study, Duvernay et al. observed formation of a $H_2$−HNCO complex from formimidic acid INT-1.[22] A multistep channel, including an initial conversion to FM, is more favorable than a one-step $H_2$ elimination (Figure 5).

(ii) Similarly, the high-energy content of the TS INT-1a-ts$H_2$ makes the 1,2-dehydrogenation from the acid INT-1a not practical. In other words, direct dissociative formation of the higher lying HOCN isomer is not competitive.

(iii) The one-step dehydrogenation from the carbene conformer INT-2b is also possible via a 1,3-$H_2$ elimination, which also yields HNCO + $H_2$. This one-step process via INT-2b-ts$H_2$ is characterized by an energy barrier of 81.3 kcal/mol, a value being ∼2.5 kcal/mol larger than that for the direct $H_2$ loss of FM via $H_2$-ts1 (78.8 kcak/mol). Within the inherent error of the methods employed on activation energies (±2.0 kcal/mol), the 1,3-$H_2$ loss can be regarded as competitive with the other dissociative process.

(iv) Overall, Figure 5 suggests that a one-step elimination of the molecular hydrogen from FM remains favored over possible multistep channels.

**c. Decarboxylation from Aminohydroxycarbene.** Of the two lower lying isomers, only the carbene can give rise to a one-step CO loss. Of the two carbene intermediates, INT-2a is the more stable (by ∼6 kcal/mol) due to the possibility for hydrogen bonding between the lone pair on the carbon with the hydrogen of the OH group.[40] Among its conformers, INT-2b disposes a suitable nuclear configuration for direct fragmentation involving INT-2b-ts$NH_3$. As shown in Figure 6, the latter TS is located at 77.2 kcal/mol, which is 3.3 kcal/mol below the position of $NH_3$-ts (80.5 kcal/mol) for one-step decarboxylation discussed above. Accordingly, the relative positions of both TSs tsH-1,2 and INT-2b-ts$NH_3$, which are both below $NH_3$-ts on the energy scale, suggest that the two-step CO-elimination channel from FM, with transient formation of the carbene isomer, competes quite favorably with the direct pathway. Within the two-step process, the rate-determining step is defined by the CO loss.

The most interesting feature of the TS INT-2b-ts$NH_3$ is that it involves a four-membered ring in which the transfer of H(OH)

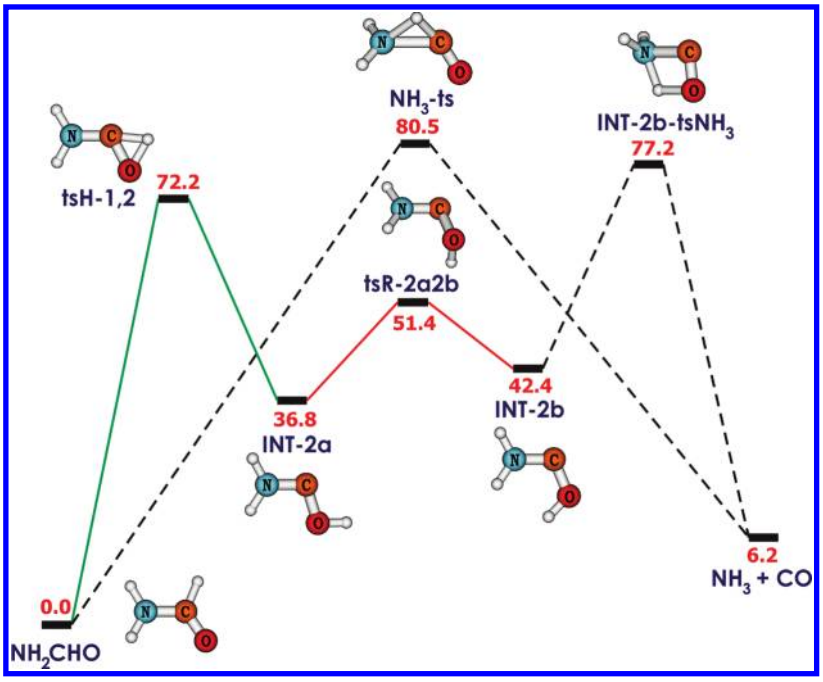


**Figure 6.** Schematic energy profiles illustrating the one-step and two-step decarbonylation of formamide. Relative energies given in kilocalories per mole are obtained from CCSD(T)/CBS + ZPE calculations.

to N is accompanied by a C−N bond cleavage. Proceeding in the opposite direction, namely, the CO + $NH_3$ addition, the CO molecule uses its $\pi$-electron system to add to an N−H bond. This is similar to a [2 + 2] cycloaddition process, in which a HOMO-$\sigma$(N−H)−LUMO-$\pi^*$(C−O) orbital interaction appears to be important. As stated above, in the TS for insertion $NH_3$-ts, CO instead uses its lone pair for a nucleophilic addition involving an n(C−O)−$\sigma^*$(N−H) orbital interaction. The [2 + 2] interaction involves a smaller orbital energy gap and as a consequence induces a stronger interaction.

Perhaps more interesting is the fact that the TS for CO loss INT-2b-ts$NH_3$ (77.2 kcal/mol) is also found to be slightly below $H_2$-ts1 (78.8 kcal/mol, Figure 2). Using RRKM calculations, the individual rate constants for the FM → ($NH_3$ + CO) and FM → INT-2a → INT-2b → ($NH_3$ + CO) channels are illustrated in Figure 3. Over all temperatures and pressures calculated, $k_3$ is greater than $k_1$ with a branching ratio ($k_3/k_1$) of ∼60 at 200 K and ∼1 at 2000 K. It can be concluded that while dehydrogenation of formamide to give $H_{2(g)}$ is basically a one-step process, decarbonylation is most likely a two-step process involving an intermediate isomer of aminohydroxycarbene. This result reconciles our calculations with the previous experiments on FM thermal decomposition that have shown the predominance of CO elimination over $H_2$ loss as discussed in section 3.1.

The behavior of aminohydroxycarbene differs from that of dihydroxycarbene, which is the carbene isomer of formic acid. It has been demonstrated that HOCOH does not participate in dehydrogenation and decarbonylation processes of HCOOH.[41]

**d. Dehydration Reactions.** As stated above, under some experimental conditions, $H_2O$ + HCN have been detected following FM thermal decomposition, along with the polymer $(HCN)_n$.[14] This prompts us to pursue the search in the regions of the [$CH_3NO$] potential energy surface describing the dehydration channels. Results of the exploration are displayed in Figure 7.

These data indicate that a single-step $H_2O$ elimination is not possible from FM. This should occur through a rearranged structure, either INT-1 or INT-2. From carbene, only one channel is open, namely, from INT-2a, which gives rise to the higher energy isomer ($H_2O$ + HNC). From INT-1c conformer, a $H_2O$-loss channel is possible, giving HCN via INT-1b-ts$H_2O$. The feature of the latter TS is mechanistically similar to that of INT-2b-ts$NH_3$. Indeed, it is a 1,2 elimination involving a $\sigma$(O−H)−$\pi^*$(C−N) interaction. In contrast, 1,1 elimination from INT-1b passing through INT-1b-ts$H_2O$ (located at 82.7 kcal/mol) is again due to formation of the lone pair of the C atom in the HNC product.

The feature of INT-1b-ts$H_2O$ has been analyzed in detail in a previous study on the HNC + $H_2O$ nucleophilic addition.[42] Of the two elimination pathways, the 1,2 loss is quantitatively favored over the 1,1 loss by ∼9 kcal/mol of the activation energy. We note that the CBS energy difference of 14.3 kcal/mol for the pair of isomer HNC−HCN (Figure 7) is quite close to the earlier theoretical results in the range of 14−15 kcal/mol.[43,44]

It is interesting that INT-1c-ts$H_2O$, located at 73.6 kcal/mol, is lower in energy than the different TSs displayed in Figures 2 and 6 for the $H_2$- and CO-loss processes. This suggests that dehydration can effectively compete with other elimination channels. While in some previous experimental studies formation of HCN was not mentioned,[11,12] in other studies a large amount of gaseous HCN was observed in a wide range of temperatures together with $NH_3$ and HNCO.[10,14] In photolysis matrix experiments, apart from the $H_2$−HNCO complex mentioned above, the HCN−$H_2O$ and HNC−$H_2O$ complexes were also characterized by IR spectrometry as primary products.[22]

RRKM calculations using the last transition state before the final products (i.e., INT-1b-ts$H_2O$ and INT-1c-ts$H_2O$ for $k_4$ and $k_5$, respectively) are employed to provide additional information about the branching ratio between the dehydration products HCN and HNC. The temperature- and pressure-dependent rate

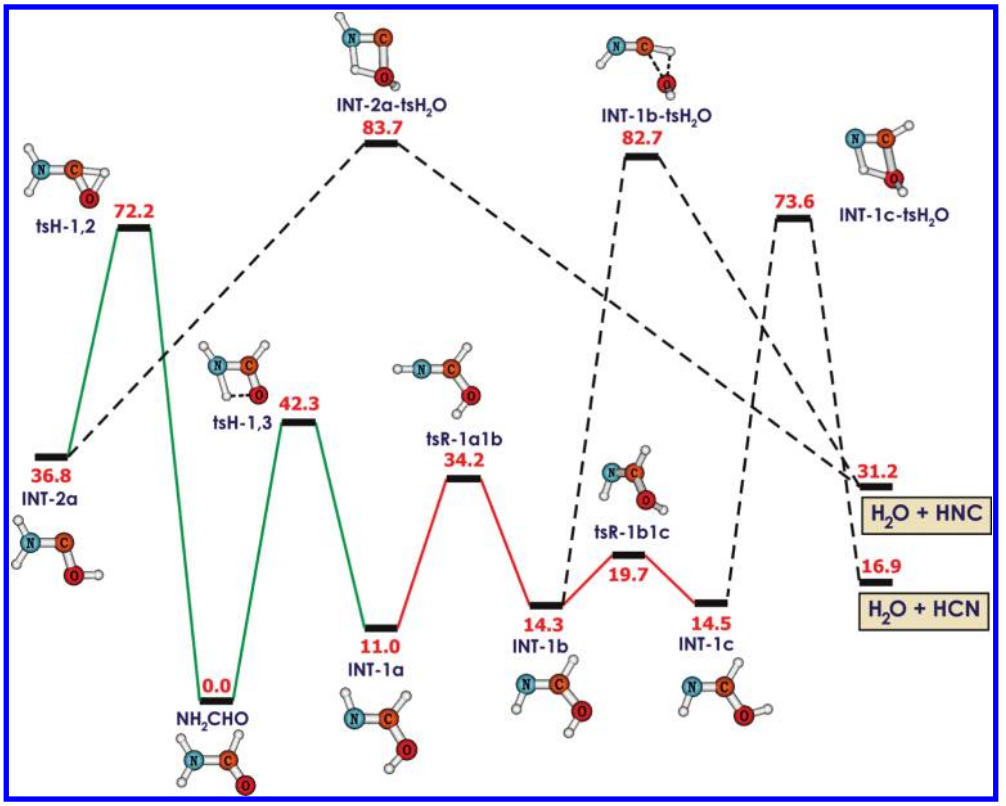


**Figure 7.** Schematic energy profiles illustrating the pathways leading to dehydration of formamide. Relative energies given in kilocalories per mole are obtained from CCSD(T)/CBS + ZPE calculations.

constants show that, over the temperature range and pressure conditions calculated, $k_5$ dominates the reactivity as compared to the other reaction pathways explored (i.e., $k_1-k_4$; see Figure 3). At the lowest temperature considered (i.e., 200 K), the branching ratio ($k_5/k_4$) is $5.22 \times 10^9$, and even at the highest temperature considered (i.e., 2000 K) $k_5$ is almost twice as probable as $k_4$ (i.e., $k_5/k_4 = 1.68$). Interestingly, RRKM calculations suggest that the multistep decomposition of formamide leading to the formation of $H_2O$ and HCN should be the dominant reaction pathway, even over the formation of $NH_3 + CO$ (cf. $k_5/k_2 = 2.69 \times 10^7$ at 200 K and $k_5/k_2 = 1.16$ at 2000 K). This $H_2O$ + HCN pathway was also recently implicated in the UV and mineral catalyzed formation of nucleobases from formamide.[9]

To verify if other isomers of FM could be involved in its decomposition, we consider the numerous stable isomers having a C−N−O skeleton. These include nitromethane ($CH_3NO$), nitrone ($CH_2NHO$), and formaldoxime ($CH_2NOH$). Dehydrogenation of these isomers could lead to other (CHNO) isomers. Dehydration is also present, in particular from formaldoxime.[45] Formation of the pair $CH_3$ + NO is also possible albeit unlikely. A crucial bridge between these two distinct regions of the energy surface is an initial conversion of FM (having N−C−O connectivity) to a C−N−O molecule. We find that such an interconversion is open via a three-membered cycle. Nevertheless, the TS connecting FM to the first ring is calculated to be at 136.6 kcal/mol above FM. The TSs for relevant processes are all situated at even higher energies. In addition, all the C−N−O isomers mentioned above are ~50 kcal/mol less stable than FM. In this context, it is likely that these isomers are not involved in FM decomposition, and therefore they are not considered further.

**e. Selected Molecular Properties of Aminohydroxymethylene.** Having established a novel mechanism for FM decarboxylation with the participation of aminohydroxymethylene INT-2, we now determine some of the characteristic properties of this transient intermediate. It is a disubstituted derivative of methylene ($CH_2$), which exhibits a triplet electronic ground state. As both amino and hydroxyl groups tend to strongly stabilize the singlet manifold, $NH_2COH$ has a singlet ground state, in the same way as the other simple hydroxycarbenes (HCOH and $CH_3COH$).[24]

So far, only the $(NH_2COH)^{+\bullet}$ radical cation has been generated by multiple mass spectrometry techniques.[15,46−48] Energetics and decomposition pathways of $(NH_2COH)^{+\bullet}$ have been determined as well by ab initio quantum chemical calculations.[49−51] Both ion isomers undergo mainly CO and $H_2$ losses. A recent mass spectrometric study of FM led to a new value for the adiabatic ionization energy of FM: $IE_{ad}$ ($NH_2CHO$) = 10.220 ± 0.005 eV.[46] This differs slightly from the currently approved value of 10.16 ± 0.06 eV, in the NIST tabulation.[52] The new value almost coincides with that of acetaldehyde, $IE_{ad}$($CH_3CHO$) = 10.229 ± 0.001 eV, and both are smaller than that of formaldehyde, $IE_{ad}(CH_2O)$ = 10.88 ± 0.01 eV.[24] For FM, a vertical counterpart, $IE_v$ = 10.42 eV has also been derived.[46] Our CCSD(T)/CBS calculations result in the values of 10.24 and 10.46 eV, respectively, that are in good agreement with the new experimental data.

During the FM mass spectrometric experiment,[46] the carbene ion isomer has not been detected, presumably due to the high-energy barrier separating both isomers. Our CBS calculations provide the values of 8.40 and 9.02 eV for the adiabatic and vertical ionization energies of $NH_2COH$, respectively. A significant

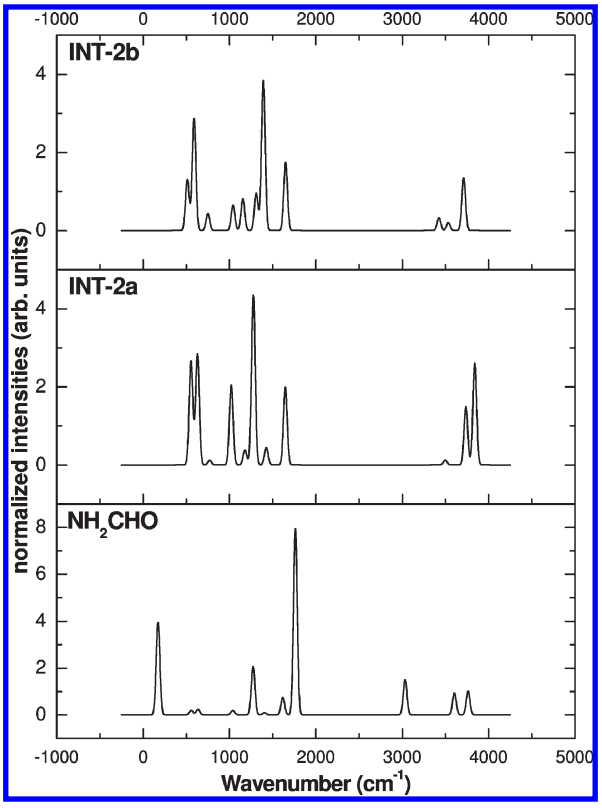


**Figure 8.** Infrared spectra of formamide and two conformers of aminohydroxymethylene plotted using vibrational frequencies and intensities computed using MP2/aug-cc-pVDZ.

relaxation of the carbene geometry thus occurs upon ionization. It is confirmed that, in the ionized form, the carbene ion $(NH_2COH)^+$ becomes the most stable isomer,[51] being ~5 kcal/mol (CBS) more stable than the FM radical cation.

Another characteristic parameter of a carbene is its singlet−triplet energy gap ($\Delta E_{ST}$). As expected, the carbene geometry is getting strongly distorted upon triplet excitation, resulting in a nearly perpendicular NCOH moiety. Such distortion is manifested in the large difference between the vertical and adiabatic $\Delta E_{ST}$ values, which amount to 78 kcal/mol (a vertical $^3A''$ state) and 58 kcal/mol for the case of $NH_2CHO$, respectively. The adiabatic gap is substantially larger than the corresponding values of 25 and 30 kcal/mol determined for HCOH and $CH_3COH$, respectively, using the same level of theory. The amino group stabilizes the singlet carbene much more strongly than the methyl. For comparison, the vertical and adiabatic $\Delta E_{ST}$ values of FM are calculated to be 124 and 98 kcal/mol, respectively; the former is close to the experimental gap of 122 kcal/mol.[53] Again, in the triplet manifold, the carbene isomer becomes more stable than FM by ~3 kcal/mol (CBS). This strongly suggests that the carbene could equally take part in a photochemical process of FM, if it occurred in a high spin state.

The vibrational spectra for the two transient carbenes, INT-2a and INT-2b, have been calculated at the MP2/aug-cc-pVDZ level, and they are shown in Figure 8. The calculated infrared spectrum of $CH_3NO$ is also shown for comparison. The vibrational signatures for INT-2a and INT-2b are similar but distinguishable from the spectrum of $CH_3NO$, which is well-established.[37,54] The calculated spectrum for the transient carbene, INT-2a, has been shown in the literature before[40] and is similar to our spectrum. As seen in Figure 8, the three structures shown have the primary NH stretches (symmetric and asymmetric) in common above 3500 $cm^{-1}$. The major difference between the carbenes and $CH_3NO$ is the lack of CH stretch vibrations at ~3000 $cm^{-1}$ in both carbene spectra, due to the hydrogen moving from carbon to oxygen in those transient species. In addition, INT-2a and INT-2b have strong C−O stretch vibrations at ~1270−1390 $cm^{-1}$ that are generally characteristic of alcohols, whereas $CH_3NO$ has a strong C═O stretch vibration at 1763 $cm^{-1}$.

## 4. CONCLUDING REMARKS

In the present theoretical study, the chemical evolution of formamide ($NH_2CHO$) is investigated using electronic structure computations. The main focus of the study is to probe the thermal decomposition mechanisms of formamide and to identify novel intermediates and reaction channels for future experimental detection. Quantum chemical calculations using the coupled cluster theory CCSD(T) whose energies are extrapolated to the complete basis set limit (CBS) are carried out to construct the $[CH_3NO]$ potential energy surface. The reactive channels leading to formation of small molecules including CO, $NH_3$, $H_2O$, HCN, HNC, $H_2$, HNCO, and HOCN are investigated.

The dehydrogenation, decarboxylation, and dehydration channels are all competitive with one another and are characterized by comparable energy barriers in the range of 73−78 kcal/mol. The $H_2$ loss favors a one-step process, although the two-step counterpart is competitive. For the CO elimination, the two-step channel involving the carbene isomer intermediate, $NH_2COH$, is clearly more favorable than the one-step channel and also more favorable than the one-step $H_2$ loss. The $H_2O$ loss from formamide is intrinsically a multistep process passing through a formimidic acid conformer, which subsequently undergoes a rate-determining dehydration. Indeed, the rate of multistep decomposition yielding $H_2O$ + HCN (i.e., $k_5$) was found to be the fastest kinetic rate with the lowest activation energy (73 kcal/mol) and largest preexponential factor ($5.69 \times 10^{13}$) over the entire temperature and pressure range explored in this work.

The exploration of formamide thermal decomposition pathways using a combination of electronic structure computations and RRKM theory provides predictions that may be informative to experimentalists studying these reactions. Dehydration of formamide to give $H_2O$ and HCN is found to be the most favorable pathway. Thus, future calculations will explore the role of water on the FM decomposition pathways and energetics by including several neighboring $H_2O$ molecules. Additionally, the presence of aminohydroxymethylene as a transient but crucial intermediate in the decarboxylation of formamide constitutes a novel feature of the reaction mechanism. Its eventual experimental detection could shed some light on the chemical transformation not only of formamide and its lower lying isomers but also of the family of carbonyl compounds.

## ■ ASSOCIATED CONTENT

**Supporting Information.** Tables with structures, rotational constants, vibrational frequencies, and total energies for all optimized geometries, the entropy, zero point correction and thermal correction for formamide, reactive intermediates, and transition states and figures of the pressure dependence of RRKM rate constants, $k_i$. This material is available free of charge via the Internet at http://pubs.acs.org.

## AUTHOR INFORMATION

### Corresponding Author

*E-mail: heather.abbott-lyon@gatech.edu (H.L.A.); minh.nguyen@chem.kuleuven.be (M.T.N.).

## ACKNOWLEDGMENT

The Leuven group is indebted to the K.U. Leuven Research Council for continuing support (GOA, IDO, and PDM programs). Authors H.L.A., M.M.D., T.M.O., and J.L. gratefully acknowledge support from the NASA Exobiology (Grant NNG05GP20G) and the NASA NAI "Titan as a Prebiotic System" grants. Additionally, this work was jointly supported by NSF and the NASA Astrobiology Program, under the NSF Center for Chemical Evolution, Grant CHE-1004570.

## REFERENCES

(1) Oparin, A. I. *The Origin of Life*; Macmillan: New York, 1938.
(2) Miller, S. L. *Science* **1953**, *117*, 528.
(3) Eschenmoser, A.; Loewenthal, E. *Chem. Soc. Rev.* **1992**, *21*, 1.
(4) Costanzo, G.; Saladino, R.; Crestini, C.; Ciciriello, F.; Di Mauro, E. *BMC Evol. Biol.* **2007**, *7*, No. S1.
(5) Gibb, E. L.; Whittet, D. C. B.; Schutte, W. A.; Boogert, A. C. A.; Chiar, J. E.; Ehrenfreund, P.; Gerakines, P. A.; Keane, J. V.; Tielens, A.; van Dishoeck, E. F.; Kerkhof, O. *Astrophys. J.* **2000**, *536*, 347.
(6) Bockelee-Morvan, D.; Lis, D. C.; Wink, J. E.; Despois, D.; Crovisier, J.; Bachiller, R.; Benford, D. J.; Biver, N.; Colom, P.; Davies, J. K.; Gerard, E.; Germain, B.; Houde, M.; Mehringer, D.; Moreno, R.; Paubert, G.; Phillips, T. G.; Rauer, H. *Astron. Astrophys.* **2000**, *353*, 1101.
(7) Raunier, S.; Chiavassa, T.; Duvernay, F.; Borget, F.; Aycard, J. P.; Dartois, E.; d'Hendecourt, L. *Astron. Astrophys.* **2004**, *416*, 165.
(8) Brucato, J. R.; Baratta, G. A.; Strazzulla, G. *Astron. Astrophys.* **2006**, *455*, 395.
(9) Barks, H. L.; Buckley, R.; Grieves, G. A.; Di Mauro, E.; Hud, N. V.; Orlando, T. M. *ChemBioChem* **2010**, *11*, 1240.
(10) Harada, K. *Nature* **1967**, *214*, 479.
(11) Back, R. A.; Boden, J. C. *Trans. Faraday Soc.* **1971**, *67*, 88.
(12) Kakumoto, T.; Saito, K.; Imamura, A. *J. Phys. Chem.* **1985**, *89*, 2286.
(13) Okazaki, M.; Funazukuri, T. *J. Mater. Sci.* **2006**, *41*, 1517.
(14) Cataldo, F.; Patane, G.; Compagnini, G. *J. Macromol. Sci., Part A: Pure Appl. Chem.* **2009**, *46*, 1039.
(15) van der Rest, G.; Mourgues, P.; Nedev, H.; Audier, H. E. *J. Am. Chem. Soc.* **2002**, *124*, 5561.
(16) Schlegel, H. B.; Gund, P.; Fluder, E. M. *J. Am. Chem. Soc.* **1982**, *104*, 5347.
(17) Nguyen, M. T.; Sengupta, D.; Vanquickenborne, L. G. *J. Phys. Chem.* **1996**, *100*, 10956.
(18) Martell, J. M.; Yu, H. T.; Goddard, J. D. *Mol. Phys.* **1997**, *92*, 497.
(19) Samuels, A. C.; Jensen, J. O.; Krishnan, P. N.; Burke, L. A. *J. Mol. Struct. (THEOCHEM)* **1998**, *427*, 199.
(20) Liu, D.; Fang, W. H.; Fu, X. Y. *Chem. Phys. Lett.* **2000**, *318*, 291.
(21) Petersen, C.; Dahl, N. H.; Jensen, S. K.; Poulsen, J. A.; Thogersen, J.; Keiding, S. R. *J. Phys. Chem. A* **2008**, *112*, 3339.
(22) Duvernay, F.; Trivella, A.; Borget, F.; Coussan, S.; Aycard, J. P.; Chiavassa, T. *J. Phys. Chem. A* **2005**, *109*, 11155.
(23) Wang, X. C.; Nichols, J.; Feyereisen, M.; Gutowski, M.; Boatz, J.; Haymet, A. D. J.; Simons, J. *J. Phys. Chem.* **1991**, *95*, 10419.
(24) Matus, M. H.; Nguyen, M. T.; Dixon, D. A. *J. Phys. Chem. A* **2006**, *110*, 8864.
(25) Matus, M. H.; Nguyen, M. T.; Dixon, D. A. *J. Phys. Chem. A* **2007**, *111*, 113.
(26) Frisch, M. J.; Trucks, G. W.; Schlegel, H. B.; Scuseria, G. E.; Robb, M. A.; Cheeseman, J. R.; Montgomery, J. A., Jr.; Vreven, T.; Kudin, K. N.; Burant, J. C.; Millam, J. M.; Iyengar, S. S.; Tomasi, J.; Barone, V.; Mennucci, B.; Cossi, M.; Scalmani, G.; Rega, N.; Petersson, G. A.; Nakatsuji, H.; Hada, M.; Ehara, M.; Toyota, K.; Fukuda, R.; Hasegawa, J.; Ishida, M.; Nakajima, T.; Honda, Y.; Kitao, O.; Nakai, H.; Klene, M.; Li, X.; Knox, J. E.; Hratchian, H. P.; Cross, J. B.; Bakken, V.; Adamo, C.; Jaramillo, J.; Gomperts, R.; Stratmann, R. E.; Yazyev, O.; Austin, A. J.; Cammi, R.; Pomelli, C.; Ochterski, J. W.; Ayala, P. Y.; Morokuma, K.; Voth, G. A.; Salvador, P.; Dannenberg, J. J.; Zakrzewski, V. G.; Dapprich, S.; Daniels, A. D.; Strain, M. C.; Farkas, O.; Malick, D. K.; Rabuck, A. D.; Raghavachari, K.; Foresman, J. B.; Ortiz, J. V.; Cui, Q.; Baboul, A. G.; Clifford, S.; Cioslowski, J.; Stefanov, B. B.; Liu, G.; Liashenko, A.; Piskorz, P.; Komaromi, I.; Martin, R. L.; Fox, D. J.; Keith, T.; Al-Laham, M. A.; Peng, C. Y.; Nanayakkara, A.; Challacombe, M.; Gill, P. M. W.; Johnson, B.; Chen, W.; Wong, M. W.; Gonzalez, C.; Pople, J. A. *Gaussian 03*; Gaussian: Wallingford, CT, 2004.
(27) Knowles, H.-J. W. P. J.; Amos, R. D.; Bernhardsson, A.; Berning, A.; Celani, P.; Cooper, D. L.; Deegan, M. J. O.; Dobbyn, A. J.; Eckert, F.; Hampel, C.; Hetzer, G.; Korona, T.; Lindh, R.; Lloyd, A. W.; McNicholas, S. J.; Manby, F. R.; Meyer, W.; Mura, M. E.; Nicklass, A.; Palmieri, P.; Pitzer, R. M.; Rauhut, G.; Schutz, M.; Stoll, H.; Stone, A. J.; Tarroni, R.; Thorsteinsson, T. *MOLPRO-2002*, a package of initio programs; University of Birmingham and Universitat Stuttgart: Birmingham, U.K., and Stuttgart, Germany, 2002.
(28) Cizek, J. *Adv. Chem. Phys.* **1969**, *14*, 35.
(29) Raghavachari, K.; Trucks, G. W.; Pople, J. A.; Head-Gordon, M. *Chem. Phys. Lett.* **1984**, 57.
(30) Dunning, T. H. *J. Chem. Phys.* **1989**, *90*, 1007.
(31) Kendall, R. A.; Dunning, T. H.; Harrison, R. J. *J. Chem. Phys.* **1992**, *96*, 6796.
(32) Peterson, K. A.; Woon, D. E.; Dunning, T. H. *J. Chem. Phys.* **1994**, *100*, 7410.
(33) Robinson, P. J.; Holbrook, K. A. *Unimolecular Reactions*; Wiley-Interscience: New York, 1972.
(34) Baer, T. *Unimolecular Reaction Dynamics: Theory and Experiments*; Oxford University Press: New York: 1996.
(35) Miller, S. L.; Urey, H. C. *Science* **1959**, *130*, 245.
(36) Troe, J. *J. Chem. Phys.* **1977**, *66*, 4758.
(37) Compilation of experimental and theoretical data available for formamide, http://cccbdb.nist.gov/exp2.asp.
(38) Sander, S. P.; Friedl, R. R.; Ravishankara, A. R.; Golden, D. M.; Kolb, C. E.; Kurylo, M. J.; Huie, R. E.; Orkin, V. L.; Molina, M. J.; Moortgat, G. K.; Finlayson-Pitts, B. J. *Chemical Kinetics and Photochemical Data for Use in Atmospheric Studies: Evaluation No. 14*; JPL Publication 02-25; National Aeronatuics and Space Administration, Jet Propulsion Laboratory, California Institute of Technology: Pasadena, CA, 2003.
(39) Maier, G.; Endres, J. *Eur. J. Org. Chem.* **2000**, 1061.
(40) Jensen, J. O.; Krishnan, P. N.; Burke, L. A. *J. Mol. Struct. (THEOCHEM)* **1996**, *370*, 245.
(41) Chang, J. G.; Chen, H. T.; Xu, S. C.; Lin, M. C. *J. Phys. Chem. A* **2007**, *111*, 6789.
(42) Nguyen, M. T.; Hegarty, A. F. *J. Chem. Soc., Perkin Trans. 2* **1987**, 1675.
(43) Sumathy, R.; Nguyen, M. T. *J. Phys. Chem.* **1998**, 8013.
(44) Nguyen, M. T.; Groarke, P. J.; Malone, S.; Hegarty, A. F. *J. Chem. Soc., Perkin Trans. 2* **1994**, 807.
(45) Heikkila, A.; Pettersson, M.; Lundell, J.; Khriachtchev, L.; Rasanen, M. *J. Phys. Chem. A* **1999**, *103*, 2945.
(46) Leach, S.; Jochims, H. W.; Baumgartel, H. *J. Phys. Chem. A* **2010**, *114*, 4847.
(47) Chamot-Rooke, J.; Mourgues, P.; van der Rest, G.; Audier, H. E. *Int. J. Mass Spectrom.* **2003**, *226*, 249.
(48) Flammang, R.; Nguyen, M. T.; Bouchoux, G.; Gerbaux, P. *Int. J. Mass Spectrom.* **2000**, *202*, A8.
(49) Ruttink, P. J. A.; Burgers, P. C.; Terlouw, J. K. *Int. J. Mass Spectrom.* **1995**, *145*, 35.
(50) Yu, D.; Armstrong, D. A.; Rauk, A. *Chem. Phys.* **1996**, *202*, 243.
(51) Bouchoux, G.; Espagne, A. *Chem. Phys. Lett.* **2001**, *348*, 329.

(52) Meierhenrich, U. J.; Munoz Caro, G. M.; Bredehoeft, J. H.; Jessberger, E. K.; Thiemann, W. H. P. *Proc. Natl. Acad. Sci. U. S. A.* **2004**, *101*, 9182.

(53) Staley, R. H.; Harding, L. B.; Goddard, W. A.; Beauchamp, J. L. *Chem. Phys. Lett.* **1975**, *36*, 589.

(54) Rubalcava, H. *Part I. The Infrared Spectra and Structure of Cyanamide. Part II. The Infrared Spectra and Structure of Formamide, N, N-dideuteroformamide, and N-methylformamide*. Ph.D. Thesis, California Insititute of Technology, Pasadena, CA, 1956.